Dynamics of CO_2 Scattering off a Perfluorinated Self-Assembled Monolayer. Influence of the Incident Collision Energy, Mass Effects, and Use of Different Surface Models[†]

Juan J. Nogueira,[‡] Saulo A. Vázquez,[‡] Oleg A. Mazyar,[§] William L. Hase,[*,§] Bradford G. Perkins, Jr.,[||] David J. Nesbitt,[||] and Emilio Martínez-Núñez[*,‡]

Departamento de Química Física, Universidad de Santiago de Compostela, 15782 Santiago de Compostela, Spain, Department of Chemistry and Biochemistry, Texas Tech University, Lubbock, Texas 79409, and JILA, University of Colorado, and National Institute of Standards and Technology, and Department of Chemistry and Biochemistry, University of Colorado, Boulder, Colorado 80309-0440

Received: November 5, 2008; Revised Manuscript Received: December 15, 2008

The dynamics of collisions of CO_2 with a perfluorinated alkanethiol self-assembled monolayer (F-SAM) on gold were investigated by classical trajectory calculations using explicit atom (EA) and united atom (UA) models to represent the F-SAM surface. The CO_2 molecule was directed perpendicularly to the surface at initial collision energies of 1.6, 4.7, 7.7, and 10.6 kcal/mol. Rotational distributions of the scattered CO_2 molecules are in agreement with experimental distributions determined for collisions of CO_2 with liquid surfaces of perfluoropolyether. The agreement is especially good for the EA model. The role of the mass in the efficiency of the energy transfer was investigated in separate simulations in which the mass of the F atoms was replaced by either that of hydrogen or chlorine, while keeping the potential energy function unchanged. The calculations predict the observed trend that less energy is transferred to the surface as the mass of the alkyl chains increases. Significant discrepancies were found between results obtained with the EA and UA models. The UA surface leads to an enhancement of the energy transfer efficiency in comparison with the EA surface. The reason for this is in the softer structure of the UA surface, which facilitates transfer from translation to interchain vibrational modes.

I. Introduction

Investigations of energy transfer and collisional accommodation between a gas and a liquid surface are of fundamental importance in acquiring a thorough comprehension of heterogeneous chemical phenomena at the molecular level. Over the last decades, advances in experimental techniques have allowed experimentalists to investigate in detail the dynamics of collisions of gases with liquid surfaces and characterize the role of important parameters, such as the mass, structure and temperature of the surface, collision energy, or impact orientation.[1−21] The quantity measured in scattering of atoms from liquid surfaces is the translational energy distribution, $P(E_f)$, of the scattered atoms, which may be determined for different polar and azimuthal angles.[3,4,20] For the scattering of a molecule such as CO_2 one may also determine its final rotational energy distribution, $P(J)$, as well as its final vibrational energies.[15−18,21]

The $P(E_f)$ and $P(J)$ distributions are often bimodal, with a low energy component that is well fit by the Boltzmann distribution for desorption at the surface temperature. It has been suggested that this component represents trapping desorption (TD) events in which the projectile may physisorb, or penetrate into the bulk liquid, and reach thermal accommodation with the surface. The high energy component of the distribution is associated with impulsive scattering (IS), for which the projectile rebounds immediately from the surface, so that the time scale of the collision is very short and insufficient for thermal equilibration with the surface. Though this is an attractive surface model, chemical dynamics simulations of projectile scattering indicate that the scattering may often be considerably more complex; e.g., direct events without trapping on the surface may scatter with a low energy Boltzmann component, often at the surface temperature, and the low energy Boltzmann component for physisorption events may have a temperature higher than that at the surface.[22−25] In addition, the forms of $P(E_f)$ and $P(J)$ may be considerably different, illustrating different collision dynamics for translational and rotational energy transfer.

One of the gas−liquid systems that has been experimentally investigated in great detail is CO_2 scattering from perfluoropolyether (PFPE).[15−18] In these experiments, carried out by Nesbitt and co-workers, supersonic jet-cooled molecular beams of CO_2 impinged on a freshly formed liquid surface of PFPE in vacuum, and the nascent internal-state distributions of the scattered CO_2 molecules were probed by high-resolution direct infrared absorption spectroscopy and laser dopplerimetry. They investigated the role of collision energy, incident angle, and surface temperature, and found that the CO_2 rotational and translational distributions are well described by the above TD + IS model, with the IS component having a Boltzmann temperature much higher than the surface temperature. The fraction of each component was found to depend significantly on collision energy and incident angle.[16,17] Also, the size of the TD component and the rotational/translational temperature of the IS component were observed to increase with surface temperature.[18]

Classical chemical dynamics simulations help to interpret experimental observations and provide additional insights into the scattering dynamics of gases with surfaces. Simulations of carbon dioxide scattering off a perfluorinated alkanethiol

---

[†] Part of the George C. Schatz Festschrift.

[*] Corresponding authors.

[‡] Departamento de Química Física, Universidad de Santiago de Compostela.

[§] Department of Chemistry and Biochemistry, Texas Tech University.

[||] JILA, University of Colorado and National Institute of Standards and Technology, and Department of Chemistry and Biochemistry, University of Colorado.

10.1021/jp809756f CCC: $40.75

[$CF_3(CF_2)_7S$] self-assembled monolayer (F-SAM) on gold, using an explicit atom (EA) model potential for the surface, gave results in quite good agreement with the scattering experiments of CO_2 + liquid PFPE, though surfaces of different nature were involved in the simulations and experiments.[18,24] This suggests that both the F-SAM and PFPE surfaces behave in similar ways in terms of energy transfer. Cooks and co-workers[26] observed similar translational to vibrational (T-V) energy transfer conversion efficiencies and, moreover, similar ion-surface reactions for both PFPE and F-SAM surfaces. These results, together with the observation of Ramasamy and Pradeep[27] that the terminal $-CF_3$ groups primarily constitute the surface of PFPE, suggest that energy transfer between the projectile and the surface is controlled by the chemical nature of the outermost layer of the surface and not by the detailed structure of the interfacial material. It is also worth mentioning that molecular dynamics simulations of long chain alkanes indicate that the liquid surface is mostly composed of the chain ends.[28] All these data strongly support the proposal that results of chemical dynamics simulations of energy transfer in collisions of gases with F-SAMs may be directly compared with the corresponding experimental information obtained for a liquid PFPE surface, provided initial conditions are chosen for the trajectories in accord with the experimental conditions. There are, however, some differences between the simulation and the experimental results, concerning the directions of the scattered CO_2 molecules, which result from the ordered structure of the F-SAM surface, as compared to the PFPE surface, and are discussed later in the paper.

The present work complements our previous simulations of CO_2 scattering off the F-SAM,[24] considering now the additional collision energies of 1.6, 4.7, and 7.7 kcal/mol and several aspects that were not investigated before. These include the influence of mass effects in the energy transfer process and the performance of a united-atom (UA) model for the F-SAM surface, in which the CF_3 and CF_2 units are represented as single pseudoatoms. This model was previously used in Ar + F-SAM simulations,[29] and it is of special interest to investigate its quality and reliability, given that this model may be very useful for large scale computations since it reduces the CPU time considerably in comparison with the explicit-atom (EA) model. A thorough comparison is made between our CO_2 + F-SAM scattering simulations and the CO_2 + PFPE scattering experiments. First, the rotational quantum number J distributions of the scattered CO_2 molecules obtained in this study are compared with the available experimental data. Second, from the projections of the velocity distributions of the scattered CO_2 molecules onto the surface plane, a translational temperature is extracted as a function of the rotational quantum number J. Experimentally, this temperature is obtained from the Doppler widths of IR laser absorption profiles of the scattered carbon dioxide molecules.

II. Computational Details

A. Potential Energy Surfaces. As in the previous work,[24] the potential energy function employed to study the dynamics of inelastic collisions of CO_2 with the F-SAM surface comprises a potential for CO_2 (V_{CO_2}), the surface potential (V_{surf}) and a CO_2/F-SAM interaction term ($V_{CO_2,surf}$):

$$V = V_{CO_2} + V_{surf} + V_{CO_2,surf} \qquad (1)$$

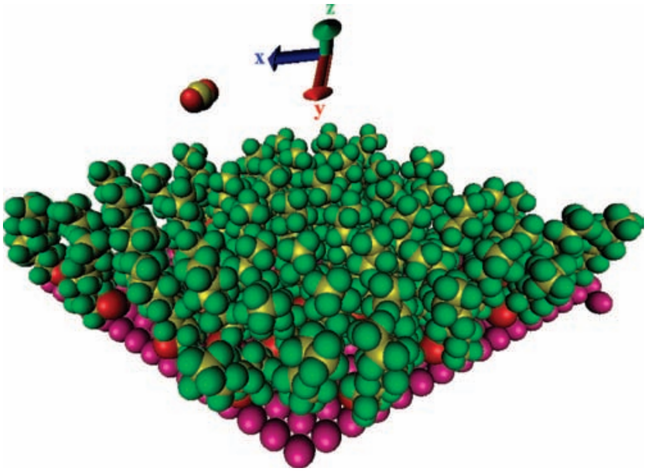

Figure 1. Snapshot of the EA model of the surface after a collision with CO_2, including the orientation of the axes considered in the present study.

We used two different models for the surface. In the explicit-atom (EA) model all atoms are treated explicitly, whereas in the united-atom (UA) model the CF_3 and CF_2 units are represented as single pseudoatoms and therefore the total number of interactions is dramatically diminished, which results in a factor of ~3 decrease in CPU time per trajectory. For both models, the F-SAM surface consists of 48 chains of $CF_3(CF_2)_7S$ radicals adsorbed on a single layer of 225 (196 in the UA model) constrained Au atoms. The details of these models were described elsewhere,[24,29] and for simplicity they are not given here. Figure 1 depicts a snapshot of the EA model of the surface after a collision with the CO_2 molecule, as well as the definition of the axes used in the simulations.

The CO_2/F-SAM interaction function ($V_{CO_2,surf}$) for the UA model was derived from a fit of the Buckingham expression to a potential, $V_{av}(R)$, obtained by isotropically averaging the EA interactions in the $CO_2 \cdots CF_4$ system:

$$V_{av}(R) = \frac{1}{n}\sum_{k=1}^{n}\sum_{i,j} V_R(r_{i,j};\theta_k, \phi_k, \chi_k) \qquad (2)$$

where R is the C$\cdots$C separation, n is the number of random orientations of CF_4 (defined in terms of the Euler angles θ_k, φ_k and χ_k) for a given distance R, and $V_R(r_{i,j};\ \theta_k,\ \varphi_k,\ \chi_k)$ is the EA potential energy of $CO_2 \cdots CF_4$. At constant R, the value of this potential energy varies with the orientation of CF_4, which determines the $r_{i,j}$ distances (i stands for C or F in CF_4 and j for C or O in CO_2). $V_{av}(R)$ is plotted in Figure 2 as circles for two different orientations of the CO_2 molecule with respect to CF_4. All points in the figure were considered in the fitting to the Buckingham potential

$$V(R) = A\exp(-BR) + C/R^D \qquad (3)$$

The parameters were obtained using a nonlinear least-squares program. To improve the computational efficiency of the simulations the value of the exponent D was rounded off to the nearest integer. After that, the remaining parameters A, B, and C were fit again fixing the value of D. The results of the fitting for the UA model are shown as a black line in Figure 2 and the parameters collected in Table 1.

B. Trajectory Simulations. The initial conditions of the trajectories were selected to model as accurately as possible the experimental conditions for CO_2 + PFPE. The angle with respect to the surface normal (z axis in Figure 1) for the CO_2 projectile, the incident polar angle (θ_i), was 0°. As in previous simulations,[24] the aiming points ($\vec{A}$) on the surface at which the CO_2 center-of-mass impacts were randomly selected by

$$\vec{A} = R_1\vec{u} + R_2\vec{v} \tag{4}$$

where the vectors $\vec{u}$ and $\vec{v}$ are determined from the Cartesian coordinates of the terminal carbon atoms for three chains at the corner of the unit cell, and R_1 and R_2 are two freshly generated random numbers. We used periodic boundary conditions and the image vector convention[30] to represent a larger surface, thus avoiding possible complications that may appear in collisions resulting in multiple CO_2 encounters with the surface.

The simulations were carried out with the VENUS05 program,[31] at collision energies (E_i) of 1.6, 4.7, 7.7, and 10.6 kcal/mol, and using both the UA and EA models; at E_i=10.6 kcal/mol only the UA model was used because the simulations with the EA model were already carried out in previous work.[24] These collision energies are the same as those used in the CO_2 + PFPE experiments, and so the present study complements our previous simulations at the collision energies of 3.0, 10.6, and 20.0 kcal/mol using the EA model.[24] The initial separation between CO_2 and the surface aiming point was 25 Å (37Å above the gold atoms). The integration of the classical equations of motion was performed with a fixed step size of 0.3 fs using the Adams-Moulton algorithm. Prior to propagation of the first trajectory, a molecular dynamics simulation was performed for 2 ps to ensure thermal relaxation of the F-SAM surface at 300 K. The structure thus obtained was used later as the initial structure of a 100 fs equilibration run before the second trajectory. This process was repeated before initiation of each trajectory.

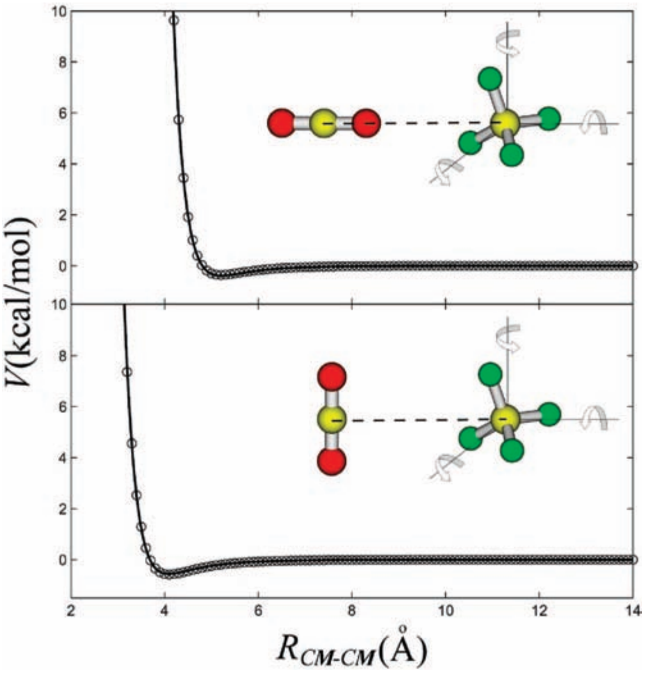

Figure 2. Two orientations between CO_2 and CF_4 used to calculate the UA model interaction potential between CO_2 and the F-SAM surface.

TABLE 1: Parameters[a] of the CO_2/F-SAM Interaction Potential

	A	*B*	*C*	*D*
	UA model			
C···CF_4	14557336.665	4.562231	− 20182460694.28	20
O···CF_4	1473656.5293	3.806771	− 11730.83989144	7
	EA model			
C···C	7560.1542982	2.913320	−502887.9228984	15
C···F	54318.344110	3.998996	−1759.413466311	8
O···C	23100.485102	3.243885	−1398.683812882	6
O···F	75993.648886	4.183596	−578.2202760926	7

[a] Units are such that the potential energy is in kcal/mol and *R* is in Å.

TABLE 2: Percentages of Trajectories That Did Not Desorb ("Incomplete" Trajectories) within the Simulation Time of 150 ps

	model	
E_i (kcal/mol)	EA	UA
1.6	3.0	38.5
4.7	2.5	30.1
7.7	1.6	23.3
10.6	0.0	22.9

Trajectories were stopped when the distance between CO_2 and the surface was 30 Å or when 150 ps elapsed. Then, the following properties were evaluated from the atomic Cartesian coordinates and momenta: the final translational and internal energy of CO_2, the final internal energy of the surface, the residence time of CO_2 (τ_{res}) on/in the surface, and the angular distributions of the scattered CO_2 atoms. Ensembles of 2000 trajectories were considered in these calculations in order to attain reasonable statistics.

For some trajectories the CO_2 molecule did not desorb during the 150 ps integration time. The percentages of these "incomplete" trajectories are collected in Table 2 for each energy and model. Almost all of the incomplete trajectories correspond to penetrating trajectories (see below for a description of the different trajectory types). The percentages of incomplete trajectories decrease with the incident energy, which is consistent with a reduction in the percentage of penetrating trajectories with collision energy (see below). In addition the percentage of incomplete trajectories is much higher for the UA model. For the incomplete trajectories, the final CO_2 translational, vibrational, and rotational energies were sampled from 300 K Boltzmann distributions and the scattering angle θ_f was randomly sampled from a cosine distribution. This is a reasonable approach because after 150 ps the CO_2 molecule is expected to reach thermal equilibrium with the F-SAM surface, so that the ensuing desorbing process will presumably proceed statistically.

III. Results

Trajectory Types. Figure 3 shows plots of the height of the CO_2 center-of-mass above the Au(111) surface as a function of time for the different trajectory types. Trajectories which move below the dashed line, which denotes the intermediate height (11.6 Å) between the average height of the C atoms of the $-CF_3$ groups and that of their adjacent $-CF_2$ groups at 300 K are identified as penetrating.[24] As seen in the plots, direct trajectories have only one inner turning point (ITP) in their perpendicular motion, whereas physisorption occurs when the molecule undergoes two or more ITPs. The time scales for both processes differ significantly, although as will be discussed later there is an important fraction of physisorbing trajectories that have just a few ITPs, and therefore their time scale is similar to that of direct trajectories. There are two types of penetrating trajectories: those that penetrate directly the surface (direct-penetration) and those that penetrate the surface after the molecule has performed several ITPs on the surface (physisorption-penetration). The time scales of the three different trajectory types (direct, physisorption, and penetration) are very different as can be seen in the

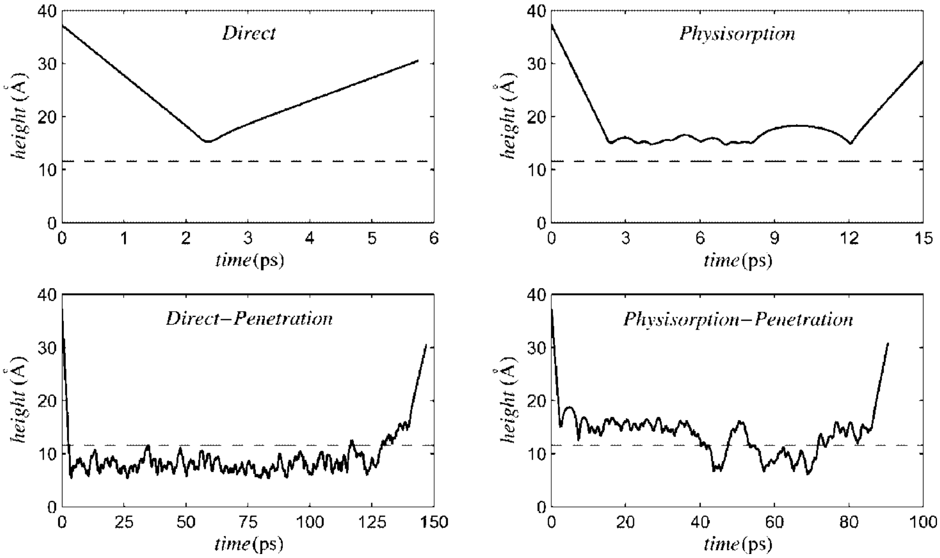

Figure 3. Variation of the CO_2 center-of-mass height with respect to the gold surface as a function of time for the different trajectory types. The plots are for typical trajectories using the EA model of the surface and E_i = 4.7 kcal/mol.

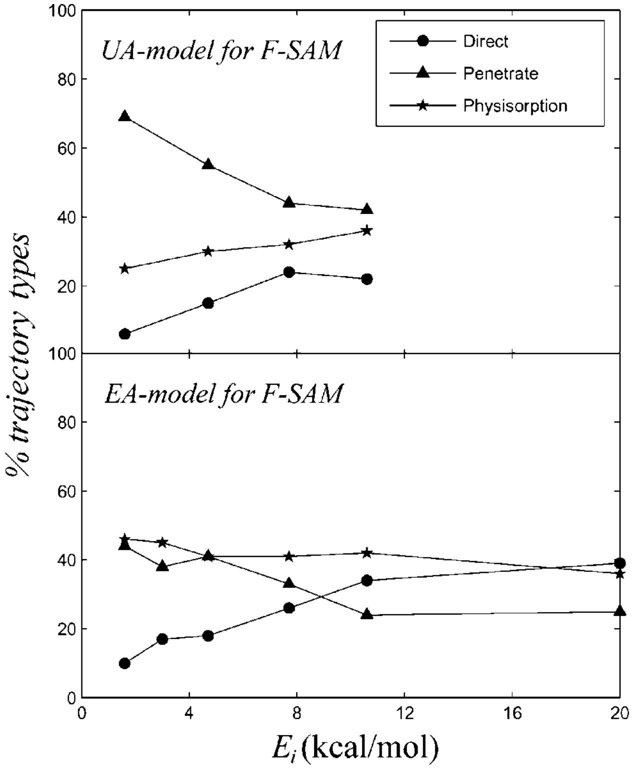

Figure 4. Percentages of different trajectory types as a function of collision energy.

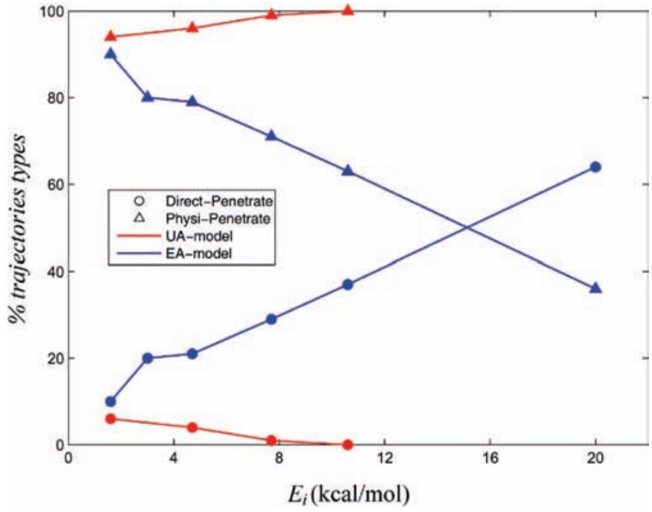

Figure 5. Percentages of direct-penetration and physisorption-penetration trajectories as a function of collision energy

plots, with the average time scale for penetrating trajectories an order of magnitude higher than those for direct trajectories.

The percentage of each trajectory type as a function of the incident collision energy is shown in Figure 4 for each surface model. The figure also collects the previous simulation results at E_i = 3.0, 10.6, and 20.0 kcal/mol for the surface EA model.[24] As seen in the plots, the percentages of trajectory types obtained with the EA surface model differ significantly from those determined with the UA model, although there are several trends that are followed by the two surface models. For example, in both cases the percentage of direct trajectories increases and the percentage of penetrating trajectories decreases with collision energy. However, the percentage of penetrating trajectories calculated with the UA model is much higher than that obtained with the EA model. Two different types of penetration trajectories were found in this study: direct-penetration, for which CO_2 molecules penetrate directly the surface and physisorption-penetration, where physisorption occurs before penetration. Figure 5 shows the percentages of direct-penetration and physisorption-penetration for both surface models as a function of collision energy. In general, the percentage of physisorption-penetration is much higher than that of direct-penetration, particularly for the UA model. On the other hand, for the UA model the percentage of physisorption-penetration increases with collision energy and the percentage of direct-penetration decreases, whereas the contrary occurs for the EA model. Actually, for the EA model at E_i = 20 kcal/mol, the percentage of direct-penetration is higher than that of physisorption-penetration. The reason for disagreement between the two surface models will be discussed in detail in a separate Section below.

Residence times. As in previous work,[24] the residence time is defined as the difference in time between the first and the last ITPs in the perpendicular motion of the CO_2 center-of-mass. With this definition, only penetrating and physisorbing trajec-

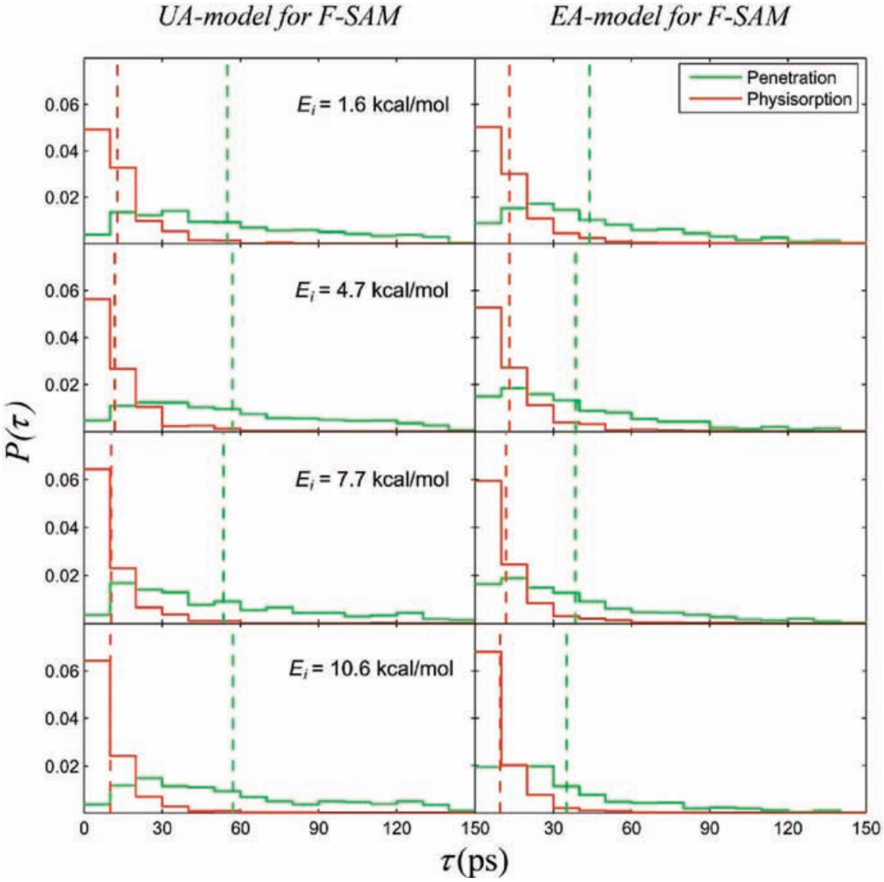

Figure 6. Distributions of residence times for physisorbing and penetrating trajectories for different collision energies. The vertical dashed lines show the average values.

tories have residence times. As found before,[24] the average residence times of penetrating trajectories are higher than those of physisorbing trajectories. At E_i = 10.6 kcal/mol, the difference between the corresponding averages is 27.0 ps for the EA surface model and 44.4 ps for the UA model. The difference is much higher for the UA model because the residence-time distributions of penetrating trajectories are much broader than those calculated with the EA model (see Figure 6). In fact, the average residence times of the physisorbing trajectories, as well as their distributions, are very similar for the EA and UA models (both show a maximum close to $\tau = 0$, and then each decreases monotonically with τ). Additionally, for the EA model the average residence times decrease with collision energy, whereas for the UA model the average values of the penetrating trajectories do not follow this trend.

Energy Transfer. Collisions of the CO_2 molecules with the F-SAM surface result in variations in the CO_2 translational energy from E_i to a final value E_f, as well as in changes in the internal energy of CO_2, ΔE_{int}, and the surface energy, ΔE_{surf}; i.e.

$$E_i = E_f + \Delta E_{int} + \Delta E_{surf} \tag{5}$$

Figure 7 gives a graphical presentation of the average percentages of E_i that go to E_f, ΔE_{int}, and ΔE_{surf}. As seen in the plots, the variations for all trajectory types follow the same pattern. In particular for ΔE_{int}, the results for all trajectory types are very similar, whereas for ΔE_{surf} and E_f there is more scattering in the results, especially at the highest energies and for the EA model. The change in the internal energy of the CO_2 molecule (ΔE_{int}) comprises a change in the vibrational and rotational energies. As in the previous simulations there is a leakage of zero-point energy from CO_2 of approximately 0.3 kcal/mol, which has been attributed to excitation of the vibrational angular momentum states of the CO_2 molecule after collision with the surface.[24] Therefore, most of the change in the internal energy of the projectile comes from rotational excitation and this excitation is relatively less important as the collision energy increases. Also seen in Figure 7 is the result that the percentage of energy transferred to the projectile's internal degrees of freedom (ΔE_{int}) does not strongly depend on the collision energy E_i, while the percentage of energy transferred to the surface ΔE_{surf} and that transferred to the translational energy of the projectile increases and decreases, respectively. The same result has been observed in previous studies,[32-35] and may be interpreted in terms of an approximate model successfully applied to collisions of gly$_2$-H$^+$ and ala$_2$-H$^+$with an F-SAM surface.[35] This model is used in the present study to analyze the energy transfer efficiencies in collisions of CO_2 with F-SAM.

The model is based on the adiabaticity parameter, ξ,[36] which is given by

$$\xi = t_c/t_v \tag{6}$$

where t_c represents the duration of the collision, which is inversely proportional to the collision velocity (v_i), and t_v is an effective vibrational period for the surface modes receiving the energy transfer. Thus, ξ is inversely proportional to the collision velocity. The average probability of energy transfer to the surface depends on ξ according to[36]

$$P_{surf}(E_i) = \frac{\langle \Delta E_{surf} \rangle}{E_i} = P_0 \exp(-\xi) = P_0 \exp(-b/v_i) \quad (7)$$

where P_0 is the limiting, small ξ, probability of energy transfer and b is a fitting parameter.

Following previous work on collisions of gly$_2$-H$^+$ and ala$_2$-H$^+$ with an F-SAM surface, we used eq. (7) to model the percentage of energy transferred to the F-SAM upon collision with CO_2 molecules, where b and P_0 are the adjustable parameters. The fitting is shown in Figure 8a and the parameters are $P_0 = 1.17$ and $b = 797$ m/s. As found before for gly$_2$-H$^+$ and ala$_2$-H$^+$ colliding with an F-SAM, P_0 is greater than unity, which is unrealistic. It has been suggested[35] that it is more appropriate to express the adiabaticity parameter, ξ, as b/E_i instead of b/v_i. The fitting for $\xi = b/E_i$ is shown in Figure 8b. As can be seen, it is apparent that the fitting is much better for $\xi = b/E_i$ than for $\xi = b/v_i$, and P_0 is now 0.86 (which is a realistic value) and $b = 2.46$ kcal/mol. The limiting energy transfer to the surface (P_0) at high energy is 86%, a value very close to the value of ~90% obtained for gly$_2$-H$^+$ and ala$_2$-H$^+$ colliding perpendicularly with F-SAM.

***P*(*J*) Distributions.** The distributions of the rotational quantum number J of the scattered CO_2 molecules are shown in Figure 9 as histograms. Each of the distributions obtained in our simulations was fit to the sum of two components: low-temperature (LT) and high-temperature (HT):

$$P(J) = \alpha_{LT} P_{LT}(J) + (1 - \alpha_{LT}) P_{HT}(J) \quad (8)$$

Each of the normalized components reads

$$P_X(J) = \frac{(2J + 1) \exp\{-E_{rot}/kT_{rot}(X)\}}{Q_{rot}(X)} \quad (9)$$

with X = LT or HT. The results of the fits are collected in Tables 3 and 4 for the UA and EA models, respectively. In some cases, the distributions were fit to a single Boltzmann distribution and α_{LT}=1, with the only variable being the rotational temperature. For the rest of the distributions the rotational temperature of the LT component was fixed to 300 K and only α_{LT} and T_{rot}(HT) were allowed to vary during the fittings; these LT and HT components are depicted in Figure 9 by lines in blue and red, respectively. This procedure is the same as that used by Nesbitt and co-workers in their experimental investigations of CO_2 + PFPE scattering dynamics,[15−18] when they referred to the LT and HT components as TD and IS, respectively.

In general the results obtained with the UA model (Table 3) are different from those obtained with the EA model of the surface (Table 4). For the penetrating trajectories and for both models $\alpha_{LT} = 1$ and the temperatures are close to 300 K, with slightly higher temperatures for the EA model of the surface. For direct and physisorption trajectories $\alpha_{LT} < 1$ for the highest collision energies, even for the UA model, although α_{LT} is always higher for the UA model than for the EA model. When all the trajectories are considered, single Boltzmann fits with $\alpha_{LT} = 1$ are obtained with the UA model for the two lowest collision energies, whereas with the EA model two Boltzmann components were obtained for all collision energies investigated.

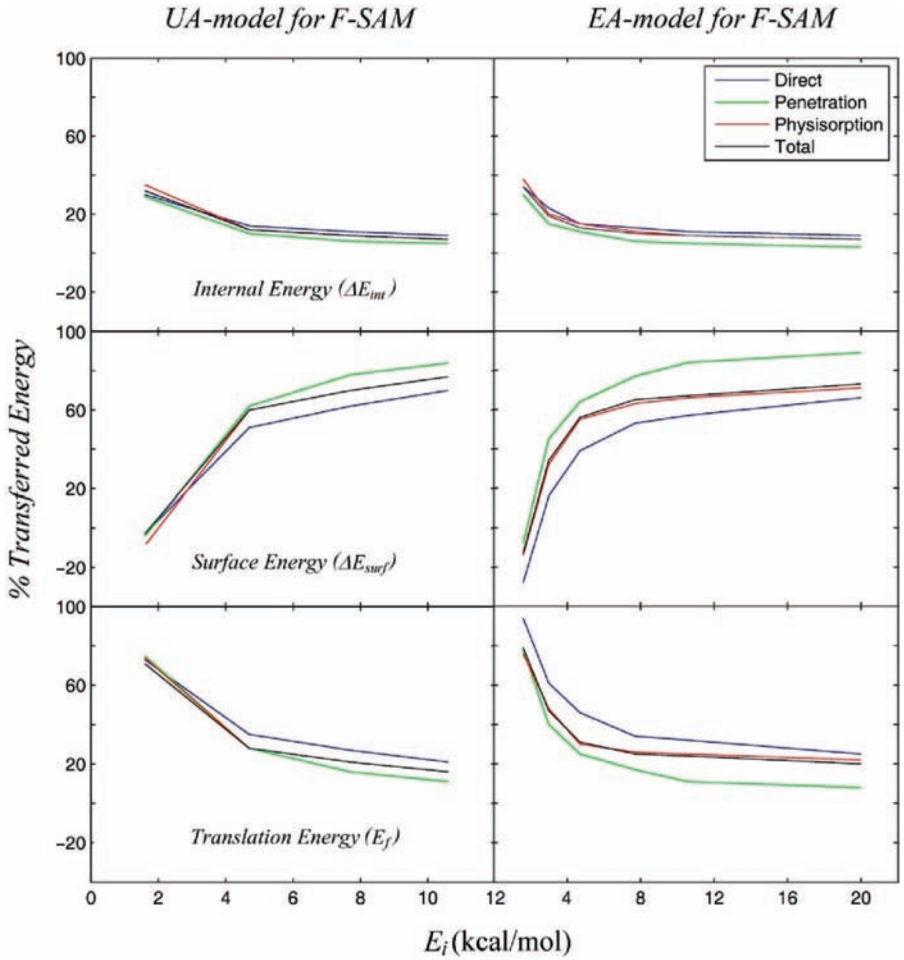

Figure 7. Average percentages of different energies (ΔE_{int}, ΔE_{surf} and E_f) as a function of collision energy for the different trajectory types.

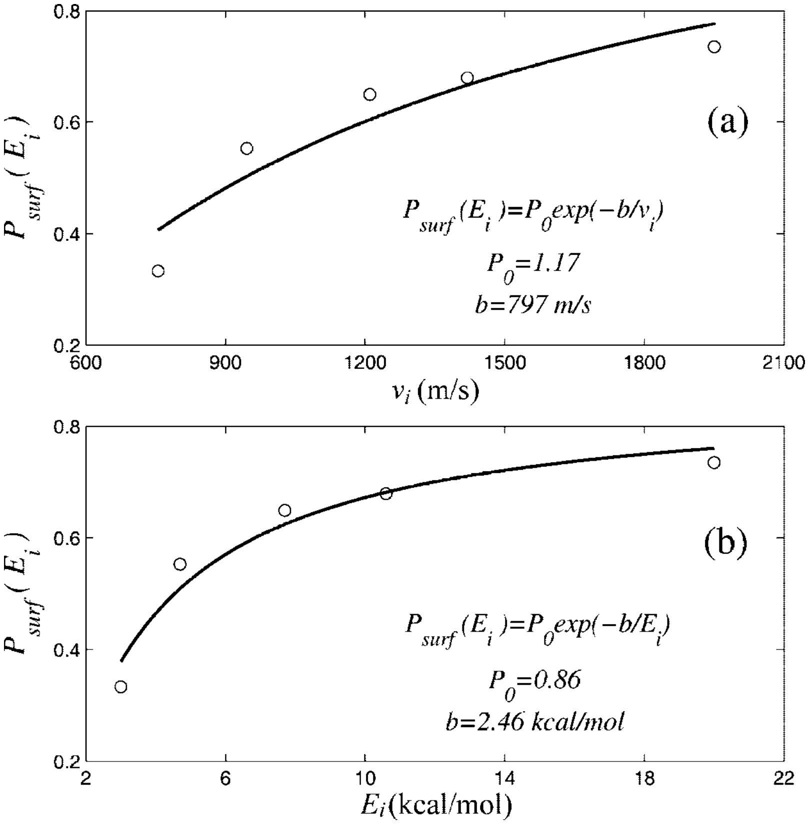

Figure 8. Fits of eq 7 to (a) the average energy transferred to the surface. In part b, the adiabaticity parameter in eq 7, ξ, was substituted by b/E_i instead of b/v_i.

A possible model for the transfer of rotational energy to CO_2 is that low values of J are associated with collisions in which CO_2 bounces multiple times at the surface, with multiple ITPs, and becomes thermally accommodated with the surface. To investigate this idea, the average number of ITPs, i.e., $\langle N_{ITPs}\rangle$, was calculated versus J for J in $\Delta J = 10$ intervals. These distributions are depicted in Figure 10 for the EA model of the surface. For the lowest collision energy $\langle N_{ITPs}\rangle$ is nearly independent of J, except for the highest J. To fit the distributions a model based on an average (constant) value for the number of ITPs for each component of the $P(J)$ distribution was used:

$$N_{\mathrm{ITPs}}(J) = \frac{1}{P(J)}\{\langle N_{ITPs}(LT)\rangle P_{LT}(J) + \langle N_{ITPs}(HT)\rangle P_{HT}(J)\} \tag{10}$$

Here $\langle N_{ITPs}(LT)\rangle$ and $\langle N_{ITPs}(HT)\rangle$ are the average number of ITPs for the LT and HT components, respectively. Using the above equation to fit the distributions (the fits are shown in Figure 10), the average number of ITPs for the LT component is 15−18 and that for the HT component is close to 0. The origin of the different dynamics for low and high E_i is uncertain and is an important topic for future studies.

Translational Energy Distributions. The final translational energy distributions $P(E_f)$ of the scattered CO_2 molecules are depicted in Figure 11 for both the UA and EA models of the surface and for different trajectory types. Usually,[3,4,12,37−45] in analyses of experiments the fraction of TD is identified as the fraction of the translational energy distribution of the scattered species, $P(E_f)$, that can be fit to a Maxwell−Boltzmann distribution for thermal desorption;[46] i.e.

$$P(E_f) = (k_BT_s)^{-2}E_f\exp(-E_f/k_BT_s) \tag{11}$$

Here k_B is Boltzmann's constant, E_f is the final translational energy of the scattered gas particle, and T_s is the surface temperature. The remaining higher energy component of the distribution is then assigned to inelastic scattering (IS). However, as will be discussed below, there are uncertainties in this approach; for instance, classical trajectory simulations of Ne scattering off SAMs adsorbed on Au(111) have shown that a Boltzmann component in $P(E_f)$ does not necessarily arise from a trapping desorption intermediate.[22,23,47,48] Therefore, in the present study we did not fit our $P(E_f)$ distributions to eq. (11). The following two-temperature Boltzmann distribution was used instead:

$$P(E_f) = \alpha_{LT}[k_BT_{trans}(LT)]^{-2}E_f\exp[-E_f/k_BT_{trans}(LT)] + (1-\alpha)[k_BT_{trans}(HT)]^{-2}E_f\exp[-E_f/k_BT_{trans}(HT)] \tag{12}$$

where, as in the $P(J)$ distributions, LT and HT are the low-temperature and high-temperature components of the distribution. The results of these fits can be compared directly with those to the $P(J)$ distributions.

The $P(E_f)$ distributions corresponding to direct trajectories in Figure 11 can not be fit with eq 12; the lines in black for these trajectories are fits obtained using the method of Legendre moments.[49] In contrast, the distributions of physisorption and penetration trajectories are fit by eq 12. The results of the fits are collected in Table 5. Penetration trajectories have $P(E_f)$ distributions that are very well fit with $\alpha_{LT} = 1$, with temperatures close to the surface temperature of 300 K for all incident energies. For physisorption trajectories at E_i of 7.7 and 10.6 kcal/mol, α_{LT} is in the range 0.30−0.52 with the temperatures of the HT component being in the range (491−847 K). For those cases in which α_{LT} is less than unity, the blue lines in Figure 11 give the LT component and the lines in red correspond to the HT component.

In general, the $P(E_f)$ distributions of physisorption trajectories and those of all the trajectories (total) are very similar to each

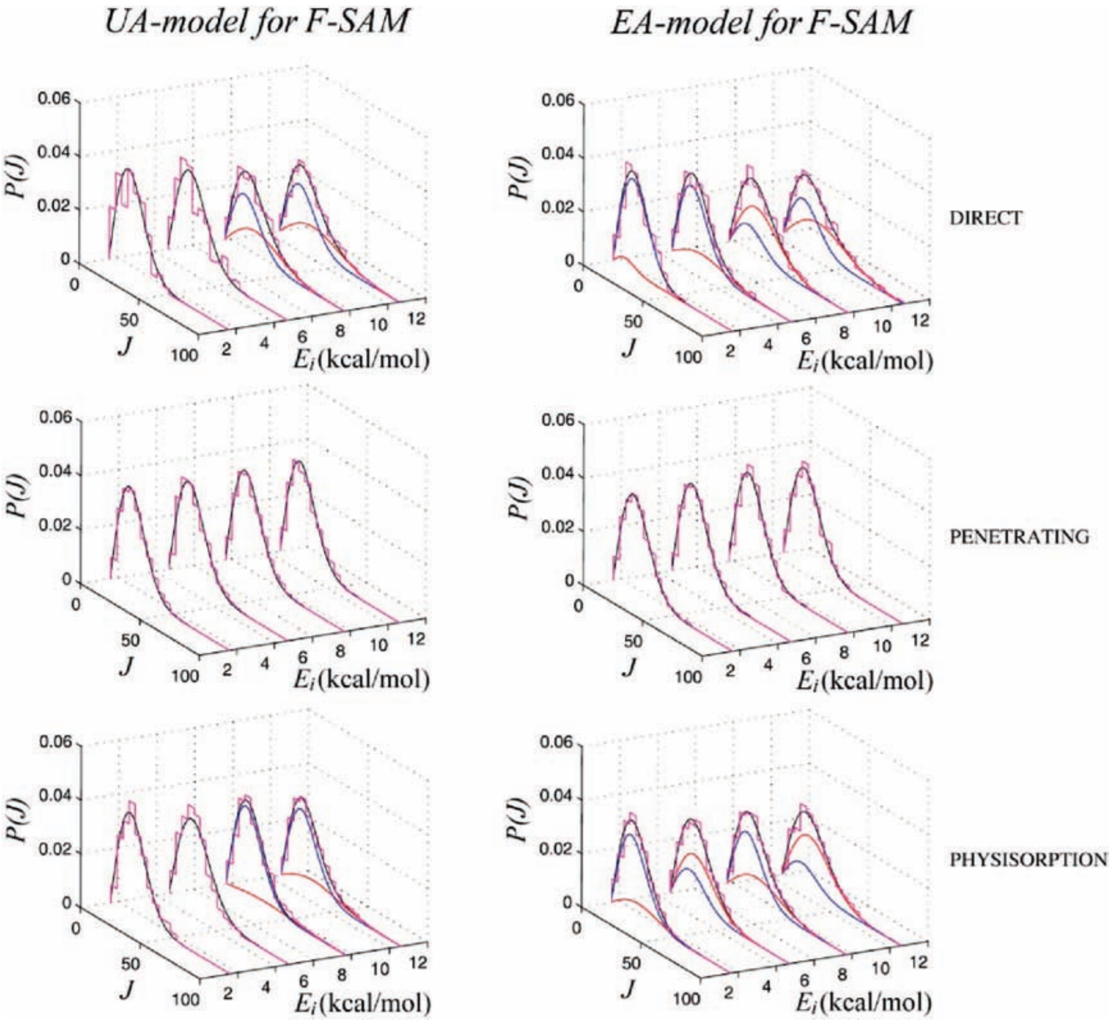

Figure 9. Distributions of the CO_2 rotational quantum number for different trajectory types as a function of the collision energy. Lines in black are fits to eq 8 (see text). When $\alpha_{LT} < 1$, the LT and HT components are shown by lines in blue and red, respectively.

other. The $P(E_f)$ distributions of penetrating trajectories peak at smaller E_f. The distributions of direct trajectories are broader and peak at much higher E_f. On the other hand, the $P(E_f)$ distributions for the EA model of the surface are much broader than those for the UA model, which is consistent with the fact that the UA model leads to more energy transfer to the surface, as indicated above, and to a lesser percentage of the high energy component in comparison with the EA model.

Percentages of Low-Temperature and High-Temperature. Figure 12 compares the fraction of LT extracted from the $P(E_f)$ distributions, $\alpha_{LT}(E_f)$, with those obtained from the analysis of the $P(J)$ distributions, $\alpha_{LT}(J)$, and with the sum of penetration and physisorption trajectories for both the UA and EA models. In general, the three fractions decrease with increasing collision energy. Exceptions occur for the UA model, as $\alpha_{LT}(E_f)$ and the sum of penetration and physisorption trajectories increase for the highest energy. In addition, the LT component becomes considerably less important at the highest E_i for the EA model.

For Ar scattering off an F-SAM surface,[29] we previously found that α_{LT} (denoted as α_{TD} in that paper) is not equivalent to either the fraction of physisorption or penetration events, or their combination. This is also observed in the present work. In a previous study of Ne scattering off SAMs by Hase and co-workers,[22,47,48] a fraction of trajectories associated with the Boltzmann component in the $P(E_f)$ distributions were found to be direct, which, to some extent, may explain the differences in Figure 12. Additionally, a fraction of trajectories associated with the high temperature component can be formed by physisorption trajectories as well. Figure 13 shows the distributions of ITPs for physisorption trajectories. As seen in the figure, all distributions peak at ITPs=2, which means that a significant fraction of physisorption trajectories may not be completely thermalized, and therefore these trajectories could be associated to the HT component. The distributions of ITPs become narrower as the collision energy increases, and an important number of physisorption trajectories have only just a few ITPs. The distributions of number of ITPs as a function of collision energy are similar for the EA and UA models, although the percentages of physisorption trajectories obtained with both models differ significantly from each other.

Scattering Angle Distributions. For each collision energy, we analyzed the distributions of the angles formed between the final CO_2 center-of-mass velocity vector and the surface normal (θ_f). These scattering angle distributions, $P(\theta_f)$, are displayed in Figure 14. The average values of the scattering angles are collected in Table 6. The dashed line in each plot of the figure is the expected distribution for random scattering ($\sin\theta\cos\theta$).[47] In only one plane perpendicular to the surface, the random distribution would be given by $\cos\theta$.[50] If we analyze separately direct, physisorbing, and penetrating trajectories, we observe clear differences between the corresponding distributions. The distributions for penetrating trajectories are more random and

TABLE 3: Parameters for the Bimodal Boltzmann Fits to the P(J) Distributions for the UA Model[a]

E_i (kcal/mol)		α_{LT}	$T_{\text{rot}}(LT)$	$T_{\text{rot}}(HT)$
		Total Trajectories		
1.6	sim.	1	282 ± 5	
	exp.[b]	0.92 ± 0.12	298	330 ± 100
4.7	sim.	1	290 ± 6	
	exp.	0.76 ± 0.07	298	520 ± 60
7.7	sim.	0.89 ± 0.03	300	1025 ± 326
	exp.	0.64 ± 0.06	298	600 ± 80
10.6	sim.	0.85 ± 0.03	300	1073 ± 315
	exp.	0.54 ± 0.03	298	710 ± 60

E_i (kcal/mol)	α_{LT}	$T_{\text{rot}}(LT)$	$T_{\text{rot}}(HT)$
	Direct Trajectories		
1.6	1	287 ± 20	
4.7	1	275 ± 15	
7.7	0.58 ± 0.10	300	723 ± 168
10.6	0.59 ± 0.08	300	864 ± 198
	Penetrating Trajectories		
1.6	1	279 ± 5	
4.7	1	284 ± 7	
7.7	1	293 ± 7	
10.6	1	291 ± 9	
	Physisorption Trajectories		
1.6	1	287 ± 12	
4.7	1	305 ± 9	
7.7	0.90 ± 0.05	300	1205 ± 882
10.6	0.78 ± 0.07	300	800 ± 273

[a] The $P(J)$ distributions are bimodal and fit with a low temperature (LT) component for thermal accommodation at the surface and a high temperature (HT) component. [b] Experimental values from ref 16.

TABLE 4: Parameters for the Bimodal Boltzmann Fits to the P(J) Distributions for the EA Model[a]

E_i (kcal/mol)		α_{LT}	$T_{\text{rot}}(LT)$	$T_{\text{rot}}(HT)$
		Total Trajectories		
1.6	sim.	0.83 ± 0.24	300	430 ± 230
	exp.[b]	0.92 ± 0.12	298	330 ± 100
4.7	sim.	0.74 ± 0.13	300	520 ± 154
	exp.	0.76 ± 0.07	298	520 ± 60
7.7	sim.	0.67 ± 0.08	300	597 ± 112
	exp.	0.64 ± 0.06	298	600 ± 80
10.6	sim.	0.52 ± 0.06	300	712 ± 78
	exp.	0.54 ± 0.03	298	710 ± 60

E_i (kcal/mol)	α_{LT}	$T_{\text{rot}}(LT)$	$T_{\text{rot}}(HT)$
	Direct Trajectories		
1.6	0.94 ± 0.13	300	120 ± 193
4.7	0.78 ± 0.14	300	713 ± 408
7.7	0.29 ± 0.15	300	585 ± 88
10.6	0.46 ± 0.06	300	933 ± 133
	Penetrating Trajectories		
1.6	1	310 ± 9	
4.7	1	302 ± 10	
7.7	1	293 ± 11	
10.6	1	313 ± 13	
	Physisorption Trajectories		
1.6	0.80 ± 0.20	300	500 ± 285
4.7	0.35 ± 0.36	300	452 ± 108
7.7	0.64 ± 0.08	300	692 ± 134
10.6	0.24 ± 0.14	300	566 ± 71

[a] The $P(J)$ distributions are bimodal and fit with a low temperature (LT) component for thermal accommodation at the surface and a high temperature (HT) component. [b] Experimental values from ref 16.

are in excellent agreement with the random scattering model. In contrast, the distributions for direct scattering are shifted toward lower θ_f and those for physisorption (shifted toward higher θ_f). This tendency becomes more pronounced as the collision energy increases.

The result that the physisorption trajectories do not follow a sin θ cos θ distribution can be explained by the fact that, as shown above (see Figure 13), a significant fraction of them have a small number of ITPs, which means that the time period of interaction with the surface is relatively small and insufficient for complete thermalization. Actually, we found here and in previous work[29] that if we increase the minimum number of ITPs in the criterion for identifying a trajectory as being of the physisorption type, the average scattering angle decreases approaching the average value of 45° for random scattering.

Distributions of the Angle Formed by the Angular Momentum of Scattered CO_2 and the Surface Normal. It is instructive to analyze whether the CO_2 molecules scatter preferentially with their angular momentum perpendicular (cartwheel type) or parallel (helicopter type) to the surface normal. Figure 15 shows the distributions of the angle β formed by the angular momentum of scattered CO_2 and the surface normal. All the distributions peak at or near 90°; that is, CO_2 scatters preferentially in a cartwheel fashion for all collision energies, trajectory types, and surface models. The vast majority of trajectories have β values in the interval 30−150°. For a CO_2 molecule to scatter in a helicopter fashion, the collision with the surface would produce a torque in the molecule with a direction parallel to the surface normal, which is very unlikely to occur. The distributions obtained with the UA model are slightly broader than those obtained with the EA model.

Mass and Surface Stiffness Effects for Energy Transfer to Hydrogenated, Fluorinated, and Chlorinated Surfaces. The importance of the mass ratio in gas−surface scattering dynamics is well documented.[50−52] Previous simulations and experiments show that hydrogenated H-SAM absorbs more energy than does the fluorinated F-SAM surface.[29,40,53] In addition, results of energy transfer in Ar + H-SAM simulations[53] agree very well with those for Ar + H/F-SAM simulations,[29] where the potential energy function is that for the F-SAM surface but the masses correspond to those of the H-SAM (with H instead of F atoms). This result indicates that it is the mass, rather than the particular details of the potential energy function, that dominates the process of energy transfer to the SAM surface.

To further investigate mass effects in collisions of gases with SAMs, we carried out two additional simulations at $E_i = 10.6$ kcal/mol, using the EA potential function. In the first simulation, the mass of the fluorine atoms was replaced by that of hydrogen, and in the second one by the mass of chlorine. These simulations will be identified as CO_2 + H/F-SAM and CO_2 + Cl/F-SAM, respectively, following the nomenclature used in our previous study.[29] Thus, the potential energy function and parameters were the same as for CO_2 + F-SAM, and the simulations only investigated a possible mass effect. The details of these simulations are the same as those described above for CO_2 + F-SAM except that the step size for the integration of the trajectories was decreased to 0.15 fs in the CO_2 + H/F-SAM simulations in order to achieve good energy conservation.

The percentage of energy transferred to the surface is 83% in the CO_2 + H/F-SAM simulations, 67% in CO_2 + F-SAM,

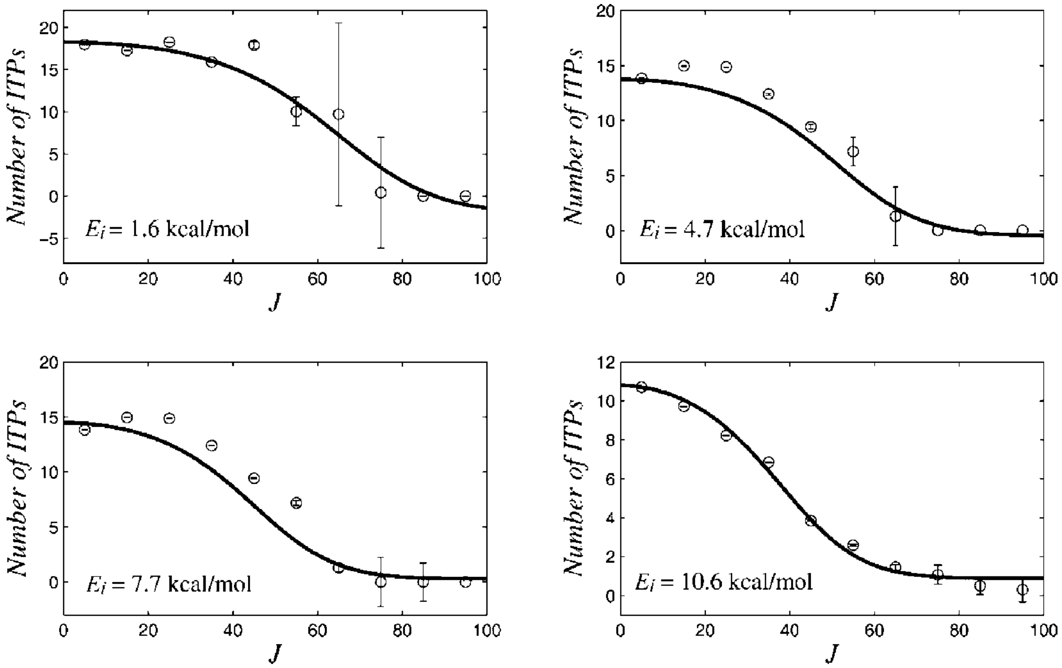

Figure 10. Distributions of inner turning points as a function of *J* for the different collision energies and for the EA model (circles) and fits of eq 10 to the distributions (solid lines).

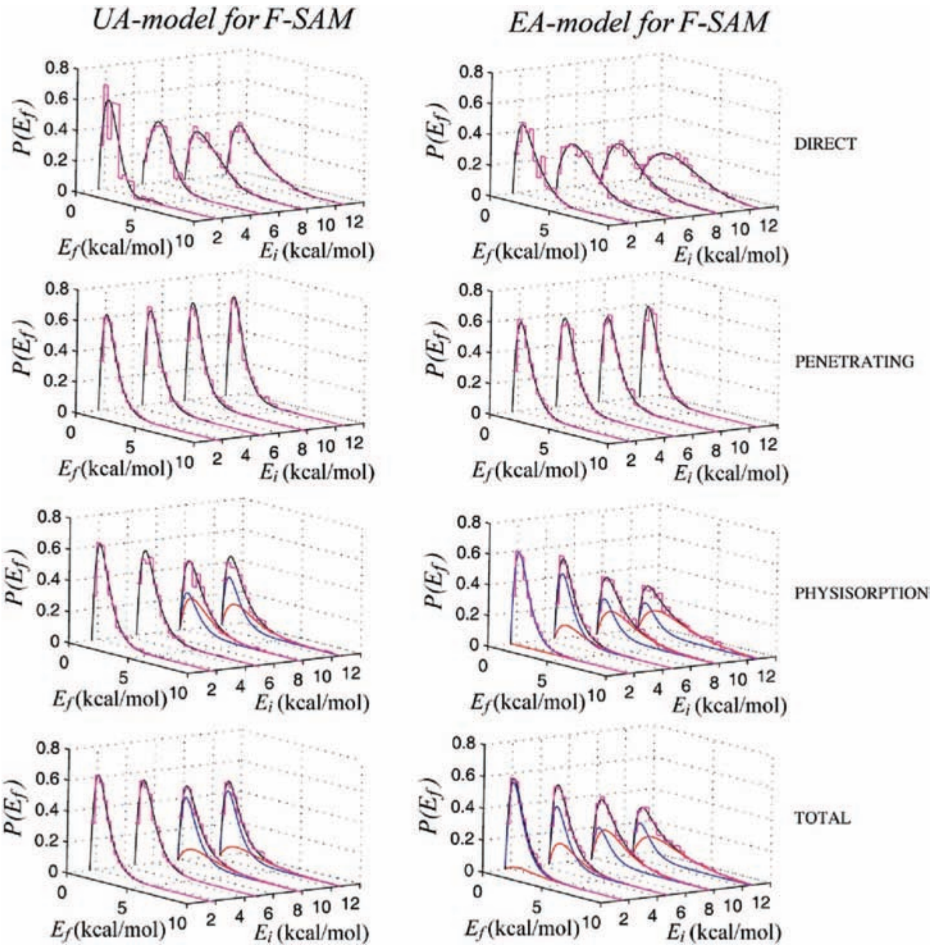

Figure 11. Distributions of the translational energy of the scattered CO_2 molecules for the different trajectory types as a function of collision energy. Histograms are the simulation results and lines are fits to Maxwell−Boltzmann distributions (see text) except for direct trajectories where the lines are Legendre fits.

and 59% in CO_2 + Cl/F-SAM. These results reproduce the experimental and simulation findings[40,53] that the hydrogenated SAM absorbs more energy than does the fluorinated one, and in turn, the F-SAM absorbs more energy than does the chlorinated surface. Additionally, our simulation results indicate that a small percentage of the initial collision energy is

TABLE 5: Parameters for the Boltzmann Fits to the P(E_f) Distributions

	united atom model			explicit atom model		
E_i (kcal/mol)	α_{LT}	$T_{\mathrm{trans}}(LT)$	$T_{\mathrm{trans}}(HT)$	α_{LT}	$T_{\mathrm{trans}}(LT)$	$T_{\mathrm{trans}}(HT)$
			Total Trajectories			
1.6	1	292 ± 1		0.91 ± 0.01	300	533 ± 31
4.7	1	326 ± 1		0.61 ± 0.01	300	484 ± 8
7.7	0.68 ± 0.01	300	630 ± 22	0.34 ± 0.01	300	593 ± 5
10.6	0.70 ± 0.01	300	686 ± 13	0.34 ± 0.00	300	861 ± 6
			Penetrating Trajectories			
1.6	1	290 ± 1		1	310 ± 1	
4.7	1	293 ± 2		1	313 ± 1	
7.7	1	284 ± 1		1	326 ± 1	
10.6	1	280 ± 2		1	305 ± 1	
			Physisorption Trajectories			
1.6	1	293 ± 1	-	0.99 ± 0.00	300	1354 ± 478
4.7	1	331 ± 1	-	0.71 ± 0.03	300	502 ± 26
7.7	0.41 ± 0.01	300	491 ± 6	0.39 ± 0.01	300	658 ± 8
10.6	0.52 ± 0.01	300	567 ± 12	0.30 ± 0.00	300	847 ± 5

transferred to the CO_2 internal degrees of freedom: 3% in the CO_2 + H/F-SAM simulations, 9% in CO_2 + F-SAM, and 10% in CO_2 + Cl/F-SAM. Most of the energy is transferred to the surface vibrational modes and, particularly, to the interchain modes of the surface, as shown in previous studies.[23,54−56] Because of the heavy mass of the alkyl chains in Cl/F-SAM and F-SAM as compared to that in H/F-SAM, the chains in the latter surface may be more mobile, which facilitates energy transfer upon collision. This effect, of decreased collisional energy transfer with decrease in surface flexibility, is consistent with a study of the Ne + H-SAM system in which energy transfer for a harmonic, single potential energy minimum model of the H-SAM was compared with that for the complete anharmonic surface model.[23] Energy transfer is less efficient for the former surface. This effect is also seen in comparing energy transfer in collisions of Ar with the H-SAM and OH-SAM. Because of hydrogen bonding the latter is less mobile.[24]

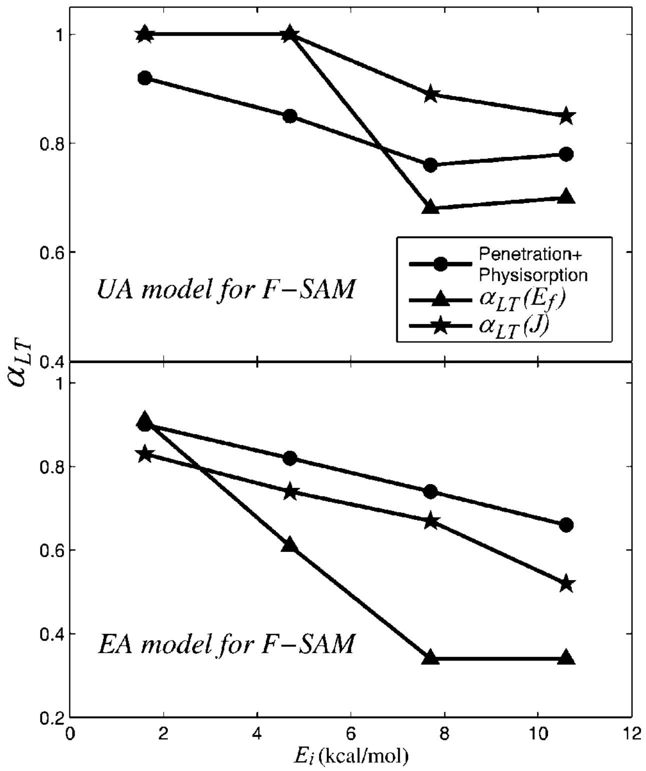

Figure 12. Variation of the trapping-desorption coefficients as a function of collision energy. These coefficients were obtained from the rotational and translational distributions and are compared in the figure with the sum of penetration and physisorption trajectories.

Comparison between the EA and UA Models of the Surface. In this study, differences between the simulation results obtained using the UA and EA models are significant and more pronounced that those found in our previous study of Ar + F-SAM collisions.[29] In the present investigation, the residence times of penetrating trajectories calculated with the UA model are markedly higher than those obtained with the EA model. Although the percentages of direct and physisorption trajectories are more or less similar in both models, the percentage of penetrating trajectories is substantially higher for the UA model of the surface (see Figure 4). For the Ar + F-SAM study, the percentages of different trajectories were essentially similar for both models at the incident energy of 100 kJ/mol although the differences for E_i = 50 kJ/mol were significant.[29]

As in previous studies of the Ar + F-SAM[29] and Ne + H-SAM systems,[48] energy transfer for the EA model is less efficient than for the UA model. Specifically, energy transferred to the EA surface was approximately 12% (10%) smaller than that transferred to the UA surface in Ar + F-SAM and Ne + H-SAM, respectively. In our CO_2 + F-SAM simulations the amount of energy transferred to the EA surface is 8−13% smaller than that in the UA model for E_i between 4.7 and 10.6 kcal/mol, in agreement with the results obtained in the Ar + F-SAM and Ne + F-SAM simulations. As mentioned above, energy is transferred preferentially to the interchain modes, and therefore the relatively less rigid structure of the UA model, which allows more conformational changes, explains why this model absorbs more collision energy than does the EA model. An increase in the nonbonded interactions between the chains in the UA model should make the chains less loosely packed, decreasing the efficiency of energy transfer to the surface. Work in our group is directed to improve the UA model of the F-SAM surface by modifying the interchain interactions. Specifically, we have modified the UA model of the surface to make it stiffer and comparable to the more realistic EA model. This work is in progress in our laboratory, and preliminary simulations with new interchain interactions in the UA model show very good agreement with EA model results.[57]

Comparison with Experiment. It is important to compare our results with experimental data of Nesbitt and co-workers.[15,16] The first comparison is for the rotational quantum number distributions *P*(*J*) of the scattered CO_2 projectiles. In previous

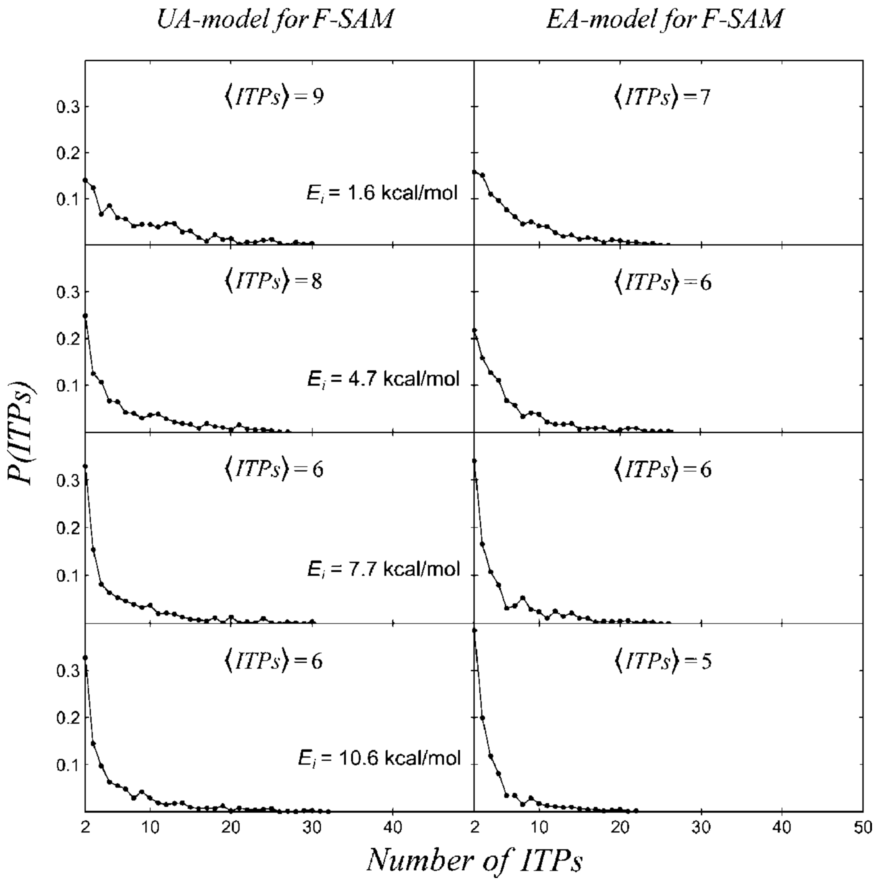

Figure 13. Distributions of inner turning points for physisorption trajectories as a function of collision energy.

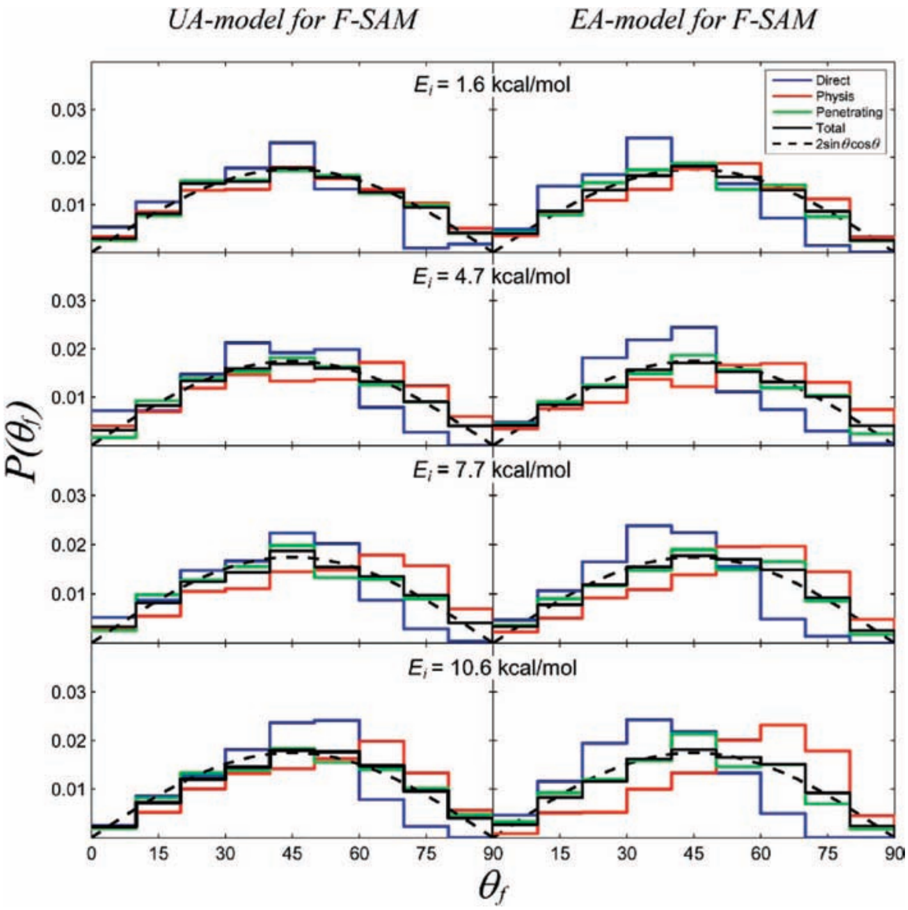

Figure 14. Distributions of the scattering angle as a function of the collision energy for the different trajectory types.

TABLE 6: Average Scattering Angles for Different Trajectory Types

E_i (kcal/mol)	direct	penetrating	physisorption	total
United Atom Model				
1.6	39.4	45.8	46.4	45.6
4.7	38.8	45.7	48.1	45.4
7.7	40.4	45.2	51.5	46.1
10.6	41.4	47.0	51.0	47.3
Explicit Atom Model				
1.6	36.7	43.6	46.8	44.4
4.7	38.0	44.6	49.9	45.6
7.7	37.1	45.0	51.9	45.8
10.6	35.6	44.1	54.7	45.8

work,[24] the $P(J)$ distribution obtained in our simulations for $E_i = 10.6$ kcal/mol was compared with the experimental one, and here we extend our previous comparison to lower incident energies. The comparison of the simulation (solid lines) and experimental (circles) $P(J)$ distributions is shown in Figure 16 for the four different collision energies. The simulation results for the total trajectories compare very well with the experimental results of Nesbitt and co-workers,[16] particularly for the EA model of the surface. For the UA model some differences become apparent as the collision energy increases, which may be associated with the fact that for this model there is no HT component, which makes the distributions narrower than the experimental (and EA) ones.

Tables 3 and 4 compare the fits of eq 8 to the simulation and experimental results. Nesbitt and co-workers fixed the LT component to 298 K in their fits, as we did for the bimodal distributions (in our case the fixed surface temperature for the bimodal distributions was 300 K instead of 298 K). For the UA model, the $P(J)$ distributions for the two lowest energies are well fit by a single Boltzmann distribution at temperatures very close to the surface temperature of 300 K. This result contrasts with the experimental fits and those for the EA-model of the surface, for which at all E_i the $P(J)$ distributions are bimodal (see Table 4). For the lowest E_i the value of α_{LT} obtained in the fit to the experimental distribution is 0.92, which is somewhat higher than that calculated in the present work (0.83); the temperatures of the HT component obtained in the fits to the experimental and simulation results are 330 and 430, respectively. For the remaining collision energies, the fitting parameters obtained with the EA model are in excellent agreement with the experimental parameters. We notice there is a difference with respect to the fitting reported in the previous simulations at $E_i = 10.6$ kcal/mol.[24] In the present case, the low temperature was not considered as a variable in the fitting, it was rather kept fixed at the surface temperature of 300 K.

The second comparison with experiment concerns the translational distributions of scattered CO_2. These were characterized and compared with the PFPE experimental results for $E_i = 10.6$ kcal/mol.[15] The high resolution detection scheme in the experiments measures CO_2 translational distributions parallel to the laser propagation direction. Each absorption profile reflects the distribution of velocities parallel to the surface. Explicitly, the Doppler profiles are fit to a Gaussian line shape to extract a characteristic translational temperature (T_{trans}) from the Doppler width, i.e.

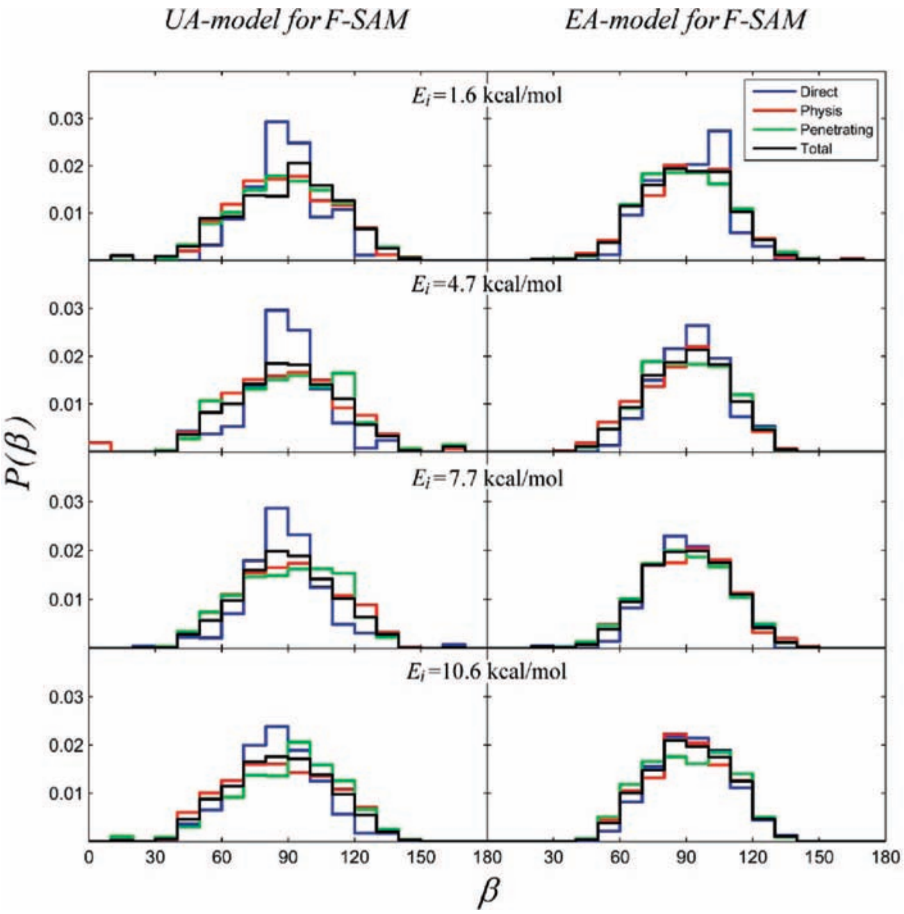

Figure 15. Distributions (per solid angle) of the angle formed by the angular momentum of the scattered CO_2 molecules and the surface normal (z axis in Figure 1) for the different trajectory types as a function of the collision energy.

$$\Delta\nu_D = 2\nu_0\sqrt{\frac{2\ln(2)\,kT_{trans}}{m_{CO_2}c^2}} \tag{13}$$

where ν_0 is the centerline rovibrational transition frequency of the asymmetric stretching mode in CO$_2$ (2419 cm^{-1} with our model potential), c is the speed of light, k is the Boltzmann constant, and m_{CO_2} the mass of the CO$_2$ molecule. Because the scattering geometry is azimuthally symmetric about the surface normal, T_{trans} characterizes both the v_x and v_y velocity distributions of the scattered CO$_2$ molecule (see Figure 1 for the definition of the x and y axes). Results from the Dopplerimetry analysis are shown in Figure 17, where T_{trans} has been plotted as a function of the J-state. Interestingly, the translational distributions broaden as J increases, which shows the surface interactions that excite CO$_2$ into high rotational states also transfer energy into translation parallel to the surface. Such a single-temperature characterization of the absorption profiles has been extended with a two-temperature line shape model that incorporates low and high temperatures along with results from the two-temperature rotational state analysis. While details of the model and fits are presented elsewhere, we plot T_{trans}(LT), T_{trans}(HT) and fit results from a predicted line shape in Figure 17 to illustrate the two-channel dynamics within the translation of scattered CO$_2$.

To compare with experimental results, the velocity distributions from the CO$_2$ + F-SAMs simulations are characterized with a similar Dopplerimetry analysis. An accurate comparison with experimental measurements involves quantum state-dependent velocity distributions that correctly account for the absorption probability associated with the laser detection scheme. In other words, the scattered flux in the simulations must be converted into a density that is based on particular velocity components of each trajectory. J-state dependent velocity distributions are generated by first sorting trajectories into $\Delta J = 10$ groups, i.e. $J = 0-10$, $10-20$, etc. Within each group, the trajectories are binned by either v_x or v_y to generate the respective velocity distribution. Instead of counting each trajectory equally within a given velocity bin, the key flux-to-density transformation weights each trajectory by the time the molecule would spend traversing across the laser beam, where the transit time is directly proportional to the probability of absorption. From the experiment configuration, we approximate the laser beam as a cylinder that passes directly above a large spot where the molecular beam strikes the surface. On the basis of this comparison, the transit time across the laser beam is proportional to $v_\perp^{-1}$, where $v_\perp = (v_x^2 + v_z^2)^{1/2}$ for v_y-distributions, and $v_\perp = (v_y^2 + v_z^2)^{1/2}$ for v_x-distributions. Resulting velocity histograms accurately simulate absorption profiles for scattered CO$_2$ that can be directly compared to the experimental Doppler profiles.

The density-based velocity distributions for the scattered trajectories once again are fit with a Gaussian line shape to extract T_{trans} along the x- and y-direction. Results of these fits are plotted in Figure 17 along with values for the CO$_2$ + PFPE experiment. Such a comparison shows nearly quantitative agreement between experiment and simulation results, where the translational distributions broaden with increasing rotational excitation. The minor discrepancy between the v_x- and v_y-distributions reflects the degree of order of the F-SAM surface, where the orientation of the terminal CF$_3$ group is different between the two directions. Such a difference is not to be expected for the PFPE liquid surface since the time-averaged motions of the surface groups randomly sample a variety of orientations. In parallel with the rotational state populations, the dynamics illustrated within the translation of scattered CO$_2$ appears to be nearly the same between the F-SAM and PFPE liquid surface, where dynamical motion of surface groups appear to be nearly the same between the two surfaces.

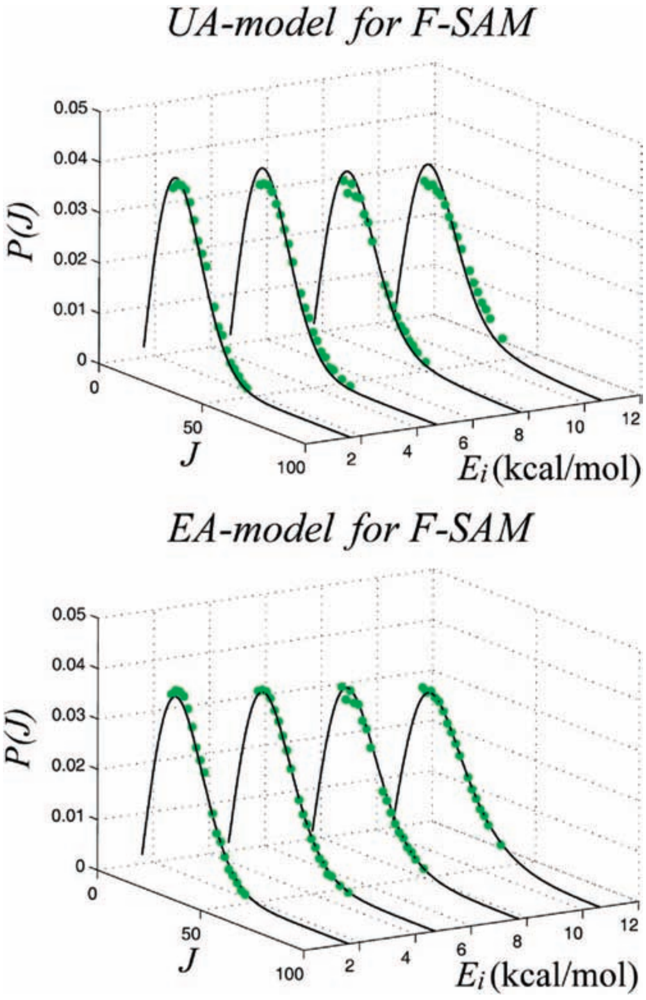

Figure 16. Distributions of the CO$_2$ rotational quantum number for total trajectories in comparison with the experimental results.[15]

IV. Conclusions

Classical trajectory calculations were carried out to further investigate the dynamics of collisions of CO$_2$ with an F-SAM on gold. The present study reports simulations for collision energies of 1.6, 4.7, 7.7, and 10.6 kcal/mol, and with the incident direction of the CO$_2$ molecules perpendicular to the surface. The results of these simulations are compared with experimental data obtained for collisions of CO$_2$ with liquid surfaces of PFPE. Although at first sight the structures of F-SAM and liquid PFPE may appear to be very different in nature, it has been shown that both surfaces exhibit similar energy transfer efficiencies as well as similar ion-surface reactions.[25] The simulations were performed with both an EA and UA model potential energy function for the F-SAM surface.

The calculations show significant differences between the results obtained with the EA model and those given by the UA model. For example, the percentage of penetrating trajectories predicted by the latter model is much higher than that calculated by the former, and the residence times of this trajectory type computed with the UA model are substantially longer than those calculated with the EA model. These results are associated with

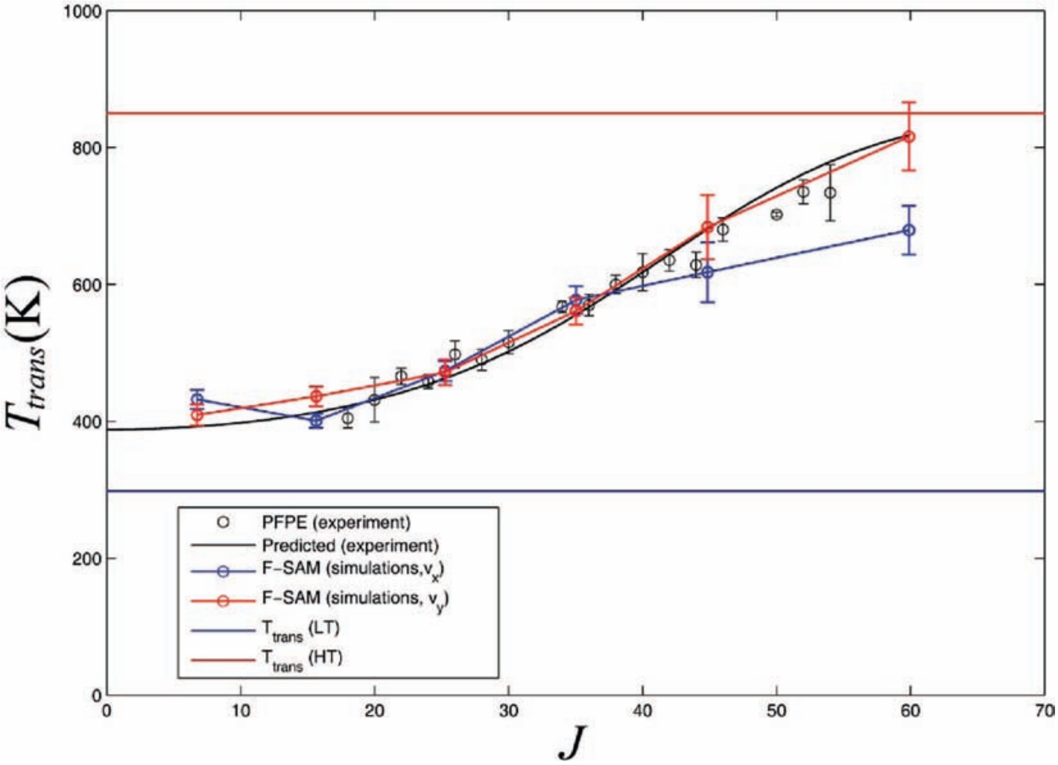

Figure 17. State-dependent translational energy distributions of scattered CO_2 for E_i=10.6 kcal/mol. Circles in blue and red give the translational temperatures corresponding to the v_x and v_y velocity distributions, respectively, as calculated by the simulations (the lines are included for visual clarity). In the experiment,[15] a single-temperature line shape gives $T_{\mathrm{trans}}(J)$, shown as black circles, while a two-temperature line shape analysis affords T_{trans}(IS), which is represented by the red horizontal line. The black line is a single Gaussian fit for a reconstructed two-temperature line shape.[15]

the fact that the UA model overestimates the efficiency of energy transfer in comparison with the EA model. Specifically, and in agreement with previous work on Ar + F-SAM and Ne + SAMs, the energy transferred to the UA surface is about 10% higher than that transferred to the EA surface. The reason for this is that the structure of the UA surface is less stiff than that of the EA surface, thus facilitating the transfer of collision energy to interchain modes. Our group is currently working on the refinement of the UA model of the F-SAM.[57] In particular, the representation of the nonbonded interaction terms in the new UA model, which have been shown to play a determinant role in energy transfer efficiencies in collisions of projectile gases with self-assembled monolayers, will be improved. As a reference, we will use the EA force field of FSAM. As in the EA model, the improved UA force fields will employ Buckingham potentials, rather than the Lennard-Jones functions utilized in the original UA model. The parametrizations will be based on fits to potential energy curves of interacting fragments (e.g., $CF_3\cdots CF_3$ or $CF_2\cdots CF_2$), calculated with the EA force field. Preliminary results[57] shows that the new UA model agrees much better with the EA model (in terms of energy transfer efficiencies, $P(J)$ and $P(E_{tr})$ distributions, etc....) for CO_2 scattering off a F-SAM surface.

The simulations corroborate the important role of the masses in the process of energy transfer. Changing the mass of the fluorine atoms by that of hydrogen or of chlorine, while keeping the parameters of the potential energy functions unchanged in order to investigate pure mass effects, we find that the efficiency of energy transfer is highest when the mass is that of hydrogen. Specifically, for E_i = 10.6 kcal/mol, the percentage of energy transferred to the surface is 83% for CO_2 + H/F-SAM collisions (mass of F atoms replaced by that of H atoms), 67% for CO_2 + F-SAM, and 59% for CO_2 + Cl/F-SAM (mass of F atoms replaced by that of Cl atoms). This trend follows the observation that energy transfer for collisions with hydrogenated SAM is more efficient than for halogenated SAMs, and may be explained by the decrease in chain flexibility as the masses of the chain atoms increase.

The rotational quantum number distributions $P(J)$ of the scattered CO_2 molecules predicted by the simulations using the EA model are in very good agreement with the corresponding experimental distributions for CO_2 + PFPE. In general, the $P(J)$ distributions for the total trajectories are bimodal, with the percentage of high temperature increasing with collision energy. For the two lowest energies, the distributions obtained with the UA model do not follow this pattern and can be fit to a single Boltzmann expression. These UA distributions differ somewhat from the experimental ones, especially as the collision energy increases. The UA distributions are slightly narrower than the experimental and EA distributions because of the lack of the high temperature component.

The translational temperatures calculated by the simulations are in quantitative agreement with those extracted from the experimental measurements. In both cases, T_{trans} increases with J. However, minor differences appear between theoretical and experimental results, where the simulations predict distinct temperatures for the v_x and v_y components. This is a consequence of the ordered structure of the F-SAM surface, which makes the x and y directions nonequivalent. In liquid PFPE, however, the random motion of the surface groups, when averaged in time, makes the x and y directions equivalent.

Acknowledgment. J.J.N, S.A.V., and E.M.-N. thank the “Ministerio de Educación y Ciencia” (Grant No. CTQ2006-

06301), “Xunta de Galicia” (Grant No. PGDIT07PXIB209072PR), and “Axuda para Consolidación e Estructuración de unidades de investigación competitivas do Sistema Universitario de Galicia, Xunta de Galicia 2007/050, cofinanciada polo FEDER 2007-2013”) for financial support. The research at Texas Tech University (TTU) is based upon work supported by the Air Force Office of Scientific Research, the Robert A. Welch Foundation under Grant No. D-0005, and the TTU High Performance Computing Center. D.J.N. and B.G.P. wish to add their grateful acknowledgement to the Air Force Office of Scientific Research for support of this work.

References and Notes

(1) Saecker, M. E.; Govoni, S. T.; Kowalski, D. V.; King, M. E.; Nathanson, G. M. *Science* **1991**, *252*, 1421.

(2) Kenyon, A. J.; McCaffery, A. J.; Quintella, C. M.; Zidan, M. D. *Chem. Phys. Lett.* **1992**, *190*, 55.

(3) Saecker, M. E.; Nathanson, G. M. *J. Chem. Phys.* **1993**, *99*, 7056.

(4) King, M. E.; Nathanson, G. M.; Hanning-Lee, M.; Minton, T. K. *Phys. Rev. Lett.* **1993**, *70*, 1026.

(5) Saecker, M. E.; Nathanson, G. M. *J. Chem. Phys.* **1994**, *100*, 3999.

(6) King, M. E.; Saecker, M. E.; Nathanson, G. M. *J. Chem. Phys.* **1994**, *101*, 2539.

(7) Nathanson, G. M.; Davidovits, P.; Worsnop, D. R.; Kolb, C. E. *J. Phys. Chem.* **1996**, *100*, 13007.

(8) King, M. E.; Fiehrer, K. M.; Nathanson, G. M.; Minton, T. K. *J. Phys. Chem. A* **1997**, *101*, 6556.

(9) Ringeisen, B. R.; Muenter, A. H.; Nathanson, G. M. *J. Phys. Chem. B* **2002**, *106*, 4988.

(10) Ringeisen, B. R.; Muenter, A. H.; Nathanson, G. M. *J. Phys. Chem. B* **2002**, *106*, 4999.

(11) Manning, M.; Morgan, J. A.; Castro, D. J.; Nathanson, G. M. *J. Chem. Phys.* **2003**, *119*, 12593.

(12) Nathanson, G. M. *Annu. Rev. Phys. Chem.* **2004**, *55*, 231.

(13) Zhang, J.; Garton, D. J.; Minton, T. K. *J. Chem. Phys.* **2002**, *117*, 6239.

(14) Kelso, H.; Kohler, S. P. K.; Henderson, D. A.; McKendrick, K. G. *J. Chem. Phys.* **2003**, *119*, 9985.

(15) Perkins, B. G., Jr.; Haeber, T.; Nesbitt, D. J. *J. Phys. Chem. B* **2005**, *109*, 16396.

(16) Perkins, B. G., Jr.; Nesbitt, D. J. *J. Phys. Chem. B* **2006**, *110*, 17126.

(17) Perkins, B. G., Jr.; Nesbitt, D. J. *J. Phys. Chem. A* **2007**, *111*, 7420.

(18) Perkins, B. G., Jr.; Nesbitt, D. J. *J. Phys. Chem. B* **2008**, *112*, 507.

(19) Zolot, A. M.; Harper, W. W.; Perkins, B. G.; Dagdigian, P. J.; Nesbitt, D. J. *J. Chem. Phys.* **2006**, *125*, 021101.

(20) Garton, D. J.; Minton, T. K.; Alagia, M.; Balucani, N.; Casavecchia, P.; Volpi, G. G. *J. Chem. Phys.* **2000**, *112*, 5975.

(21) Perkins, B. G., Jr; Nesbitt, D. J. *Proc. Natl. Acad. Sci. U.S.A.* **2008**, *105*, 12684.

(22) Yan, T.; Hase, W. L.; Barker, J. R. *Chem. Phys. Lett.* **2000**, *329*, 84.

(23) Yan, T.; Isa, N.; Gibson, K. D.; Sibener, S. J.; Hase, W. L. *J. Phys. Chem. A* **2003**, *107*, 10600.

(24) Martínez-Núñez, E.; Rahaman, A.; Hase, W. L. *J. Phys. Chem. C* **2007**, *111*, 354.

(25) Tasic, U.; Day, B. S.; Yan, T.; Morris, J. R.; Hase, W. L. *J. Phys. Chem. C* **2008**, *112*, 476.

(26) Pradeep, T.; Miller, S. A.; Cooks, R. G. *J. Am. Soc. Mass Spectrom.* **1993**, *4*, 769.

(27) Ramasamy, S.; Pradeep, T. *J. Chem. Phys.* **1995**, *103*, 485.

(28) Harris, J. G. *J. Phys. Chem.* **1992**, *96*, 5077.

(29) Vazquez, S. A.; Morris, J. R.; Rahaman, A.; Mazyar, O. A.; Vayner, G.; Addepalli, S. V.; Hase, W. L.; Martinez-Nunez, E. *J. Phys. Chem. A* **2007**, *111*, 12785.

(30) Allen, M. P.; Tildesley, D. J. Computer Simulation of Liquids; Clarendon Press: Oxford, 1987.

(31) VENUS05 is an enhanced version of VENUS96, with additional algorithms. VENUS96 is available on the website cdssim.chem.ttu.edu and was initially released through: *QCPE Bull.* **1996**, *16*, 671.

(32) Meroueh, O.; Hase, W. L. *J. Am. Chem. Soc.* **2002**, *124*, 1524.

(33) Wang, J.; Meroueh, S. O.; Wang, Y.; Hase, W. L. *Int. J. Mass. Spectrom.* **2003**, *230*, 57.

(34) Song, K.; Meroueh, O.; Hase, W. L. *J. Chem. Phys.* **2003**, *118*, 2893.

(35) Yang, L.; Mazyar, O. A.; Lourderaj, U.; Wang, J.; Rodgers, M. T.; Martinez-Nunez, E.; Addepalli, S. V.; Hase, W. L. *J. Phys. Chem. A* **2008**, submitted.

(36) Levine, R. D.; Bernstein, R. B. *Molecular Reaction Dynamics and Chemical Reactivity*; Oxford University Press: New York, 1987.

(37) Cohen, S. R.; Naaman, R.; Sagiv, J. *Phys. Rev. Lett.* **1987**, *58*, 1208.

(38) Paz, Y.; Naaman, R. *J. Chem. Phys.* **1991**, *94*, 4921.

(39) Day, B. S.; Morris, J. R. *J. Phys. Chem. B* **2003**, *107*, 7120.

(40) Gibson, K. D.; Isa, N.; Sibener, S. J. *J. Chem. Phys.* **2003**, *119*, 13083.

(41) Day, B. S.; Shuler, S. F.; Ducre, A.; Morris, J. R. *J. Chem. Phys.* **2003**, *119*, 8084.

(42) Hwang, G. S.; Anderson, C. M.; Gordon, M. J.; Moore, T. A.; Minton, T. K.; Giapis, K. P. *Phys. Rev. Lett.* **1996**, *77*, 3049.

(43) Minton, T. K.; Giapis, K. P.; Moore, T. *J. Phys. Chem. A* **1997**, *101*, 6549.

(44) Hurst, J. E.; Becker, C. A.; Cowin, J. P.; Janda, K. C.; Wharton, L.; Auerbach, D. J. *Phys. Rev. Lett.* **1979**, *43*, 1175.

(45) Rettner, C. T.; Schweizer, E. K.; Mullins, C. B. *J. Chem. Phys.* **1989**, *90*, 3800.

(46) Grimmelmann, E. K.; Tully, J. C.; Cardillo, M. J. *J. Chem. Phys.* **1980**, *72*, 1039.

(47) Yan, T.; Hase, W. L. *Phys. Chem. Chem. Phys.* **2000**, *2*, 901.

(48) Yan, T.; Hase, W. L. *J. Phys. Chem. B* **2002**, *106*, 8029.

(49) Aoiz, F. J.; BanÌares, L. *J. Phys. Chem.* **1996**, *100*, 18108.

(50) Goodman, F. O.; Wachman, H. Y. *Dynamics of Gas-Surface Scattering*; Academic Press: New York, 1976.

(51) Harris, J. Mechanical Energy Transfer in Particle-Surface Collisions. In *Dynamics of Gas-Surface Interactions*; Rettner, C. T., Ashfold, M. N. R., Eds.; Royal Society of Chemistry: Cambridge, U.K., 1991.

(52) Szabo, T. J.; Siavosh-Haghighi, A.; Adams, J. E. *J. Phys. Chem. B* **2006**, *110*, 1319.

(53) Day, B. S.; Morris, J. R.; Troya, D. *J. Chem. Phys.* **2005**, *122*, 214712.

(54) Isa, N.; Gibson, K. D.; Yan, T.; Hase, W.; Sibener, S. J. *J. Chem. Phys.* **2004**, *120*, 2417.

(55) Yan, T.; Hase, W. L. *J. Phys. Chem. A* **2001**, *105*, 2617.

(56) Yan, T.; Hase, W. L.; Tully, J. C. *J. Chem. Phys.* **2004**, *120*, 1031.

(57) Nogueira, J. J.; Martinez-Nunez, E.; Vazquez, S.;*J. Phys. Chem. C (submitted).*

JP809756F